MAGNETIC RESONANCE IN CHEMISTRY
Magn. Reson. Chem. 2005; **43**: S130–S139
Published online in Wiley InterScience (www.interscience.wiley.com). DOI: 10.1002/mrc.1689

High-frequency/high-field EPR spectroscopy of the high-spin ferrous ion in hexaaqua complexes†

Joshua Telser,[1] Joris van Slageren,[2] Suriyakan Vongtragool,[2] Martin Dressel,[2] William M. Reiff,[3] S. A. Zvyagin,[4] Andrew Ozarowski[5] and J. Krzystek[5]*

[1] Chemistry Program, Roosevelt University, Chicago, IL 60605, USA
[2] 1. Physikalisches Institut, Universität Stuttgart, Pfaffenwaldring 57, D-70550 Stuttgart, Germany
[3] Department of Chemistry and Biochemistry, Northeastern University, Boston, MA 02115, USA
[4] Hochfeld-Magnetlabor Dresden, Forschungszentrum Rossendorf, D-01328 Dresden, Germany
[5] National High Magnetic Field Laboratory, Tallahassee, Florida 32310, USA

Received 31 March 2005; Revised 7 June 2005; Accepted 10 June 2005

Electron paramagnetic resonance (EPR) at conventional magnetic fields and microwave frequencies, respectively, $B_0 \leq 1.5$ T, $\nu \leq 35$ GHz, has been widely applied to odd electron-number ($S = 1/2$) transition metal complexes. This technique is less successfully applied to high-spin systems that have even electron configurations, e.g. Fe^{2+} ($S = 2$). The recently developed technique of high-frequency and high-field EPR (HFEPR), employing swept fields up to 25 T combined with multiple, sub-THz frequencies readily allows observation of EPR transitions in such high-spin systems. A parallel spectroscopic technique is frequency-domain magnetic resonance spectroscopy (FDMRS), in which the frequency is swept while at zero, or at discrete applied magnetic fields. We describe here the application of HFEPR and FDMRS to two simple high-spin (HS) ferrous (Fe^{2+}) salts: ferrous perchlorate hydrate, $[Fe(H_2O)_6](ClO_4)_2$ and $(NH_4)_2[Fe(H_2O)_6](SO_4)_2$, historically known as *ferrous ammonium sulfate*. Both compounds contain hexaaquairon(II). The resulting spectra were analyzed using a spin Hamiltonian for $S = 2$ to yield highly accurate spin-Hamiltonian parameters. The complexes were also studied by powder DC magnetic susceptibility and zero-field Mössbauer effect spectroscopy for corroboration of magnetic resonance results. In the case of $[Fe(H_2O)_6](ClO_4)_2$, all the magnetic techniques were in excellent agreement and gave as consensus values: $D = 11.2(2)$ cm^{-1}, $E = 0.70(1)$ cm^{-1}. For $(NH_4)_2[Fe(H_2O)_6](SO_4)_2$, FDMRS and HFEPR gave $D = 14.94(2)$ cm^{-1}, $E = 3.778(2)$ cm^{-1}. We conclude that the spin-Hamiltonian parameters for the perchlorate best represent those for the isolated hexaaquairon(II) complex. To have established electronic parameters for the fundamentally important $[Fe(H_2O)_6]^{2+}$ ion will be of use for future studies on biologically relevant systems containing high-spin Fe^{2+}. Copyright © 2005 John Wiley & Sons, Ltd.

KEYWORDS: iron(II); ferrous complexes; electron paramagnetic resonance; high-field/high-frequency EPR; HFEPR; frequency-domain magnetic resonance; FDMRS; Mossbauer effect spectroscopy, zero-field splitting

INTRODUCTION

Electron paramagnetic resonance (EPR) spectroscopy has been extensively used to investigate a wide variety of complexes of the transition metal (3d block) ions. From a biological point of view,[1,2] perhaps the most important among the many 3d block ions are the two most commonly found for iron: Fe^{3+} (ferric ion, $3d^5$) and Fe^{2+} (ferrous ion, $3d^6$). Depending on the ligand-field strength and symmetry of the coordination environment, a ferrous ion can be in either the high-spin (HS, $S = 2$) or low-spin (LS, $S = 0$) electronic configuration or more rarely the intermediate spin $S = 1$. The LS ground state is diamagnetic, so no form of paramagnetic resonance is applicable, but EPR is possible at least in principle for the HS ground state. In practice, however, conventional EPR of HS Fe^{2+} can either be impossible ('EPR-silent' system) or difficult and/or uninformative, unless the symmetry is very high (cubic).

The experimental difficulty of EPR of HS Fe^{2+} in reduced symmetry environments results from anisotropic orbital angular momentum contributions, which cause zero-field splitting (zfs) that partially removes the degeneracy of the $\langle S, M_S|$ levels, even in the absence of an applied magnetic field. The resulting splitting is shown in Fig. 1. It can be seen that if in an axial coordination environment the energy separation given by D is larger than $h\nu$ (the microwave quantum; $\sim$0.3 cm^{-1} at X-band), then there will be generally no observable EPR transitions under conventional experimental conditions. A symmetry lower than axial introduces a

†**Presented as part of a special issue on High-field EPR in Biology, Chemistry and Physics.**

*Correspondence to: J. Krzystek, National High Magnetic Field Laboratory, Florida State University, 1800 E. Paul Dirac Dr, Tallahassee, FL 32310, USA. E-mail: krzystek@fsu.edu

Contract/grant sponsor: National Science Foundation, the W. M. Keck Foundation and German Science Foundation; Contract/grant number: DMR 0084173.

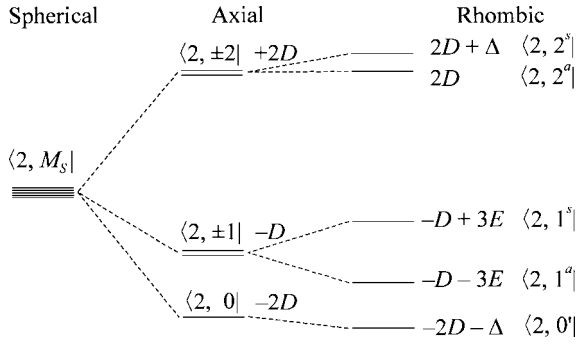

Figure 1. Energy diagram for an $S = 2$ system undergoing axial zero-field splitting (positive D), and with additional rhombic zero-field splitting ($E \neq 0$). $\Delta = 3E^2/D$. In the rhombic case, an EPR transition (often referred to as the 'non-Kramers transition') between the states labeled $\langle 2, 2^a|$ and $\langle 2, 2^s|$ is partially allowed. When D is negative, these two states are lowest in energy and the non-Kramers transition is sometimes observable at low fields and frequencies. Its intensity is enhanced by use of parallel mode microwave polarization.

rhombic zfs term, E. As shown in Fig. 1, this leads to a further splitting of the $\langle S, M_S| = \langle 2, \pm 2|$ levels, with the splitting given (in the second-order perturbation calculation) by $\Delta = 3E^2/D$. It is sometimes possible to employ EPR at conventional frequencies to observe a nominally forbidden ($\Delta M_S = 4$, enhanced in parallel mode EPR) transition between these two, which usually occurs at a very low (nearly zero) applied magnetic field. This 'non-Kramers' transition has been productively investigated in recent years in certain HS Fe^{2+} systems.[3] For further discussion of the non-Kramers transition, we refer the reader to the work of Hendrich and co-workers.[3,4]

The above summarizes the situation regarding EPR of HS Fe^{2+} prior to the introduction of a powerful new electron magnetic resonance technique: high-frequency and high-field EPR (HFEPR).[5–8] As currently practiced, by us and others,[9] this technique employs high fields, in our case up to 25 T, in combination with multiple energy sources in the sub-THz range. The experimental aspects of HFEPR are outside the scope of this paper; the key points for HS Fe^{2+}, however, are that (i) the Zeeman effect of the high fields raises the energy of lower-lying M_S levels while lowering the energy of higher-lying M_S levels so that allowed transitions among these levels can be observed experimentally, and (ii) the large energy quantum further permits many of these allowed transitions to be observed. The advantages of HFEPR will be specifically demonstrated below for two complexes of HS Fe^{2+}, particularly in its tunable-frequency version, which allows the resonances to be followed quasi-continuously as a function of the energy quantum.

Another experimental technique that has been successfully employed to investigate magnetic properties of HS species such as HS Fe^{2+} is frequency-domain magnetic resonance spectroscopy (FDMRS). This method was actually introduced quite early on;[10–12] however, it was discontinued for several decades, presumably because of low sensitivity and other technical problems. It is only in recent years that this technique was reintroduced[13,14] into the armamentarium of experimental methods well suited for investigating HS transition metal ions and their clusters. This renaissance is credited to the availability of voltage-controlled tunable-frequency sub-THz and low-THz wave sources, called *backward-wave oscillators* (BWOs). FDMRS depends on sweeping the frequency either in a zero field, or in a fixed magnetic field. As such, it is equivalent to HFEPR, which depends on continuously sweeping the magnetic field, while holding the sub-THz frequency fixed for the given spectrum. In this work, we discuss how these two techniques complement each other in the case of HS Fe^{2+}.

As mentioned at the outset, complexes containing Fe ions are of great interest from a bioinorganic chemistry point of view. Some of us have previously reported a HFEPR study of a four-coordinate complex of Fe^{2+}, $(PPh_4)_2[Fe(SPh)_4]$ (Ph = phenyl), which is a model for the reduced form of the mononuclear iron–sulfur protein, rubredoxin.[15] The electronic ground state of such a pseudo-tetrahedral $3d^6$ complex is similar to that of a pseudo-octahedral $3d^4$ complex such as those of Mn^{3+}, which have been extensively studied by HFEPR.[9,16–24] In contrast, HFEPR spectra of pseudo-octahedral HS Fe^{2+} have proven elusive, despite intensive efforts by ourselves, and presumably others. Very recently, some of us have reported a HFEPR study of a six-coordinate complex of HS Fe^{2+} in a relatively low symmetry environment and with rather elaborate ligands as in bis(2,2′-bi-2-thiazoline)bis(isothiocyanato)iron(II), $[Fe(btz)_2(SCN)_2]$.[25] A simpler six-coordinate complex of HS Fe^{2+}, $[Fe(imidazole)_6](NO_3)_2$, had been studied by HFEPR the previous year.[26] However, the main thrust of that work was an extensive inelastic neutron scattering (INS) study. Indeed, it appears that good-quality HFEPR spectra for octahedral Fe(II) are exceptions rather than the rule, which leaves many open questions such as whether this system can or cannot be interpreted using the standard $S = 2$ spin-Hamiltonian formalism. It has thus been the main objective of this work to show that informative HFEPR spectra can be obtained despite numerous experimental difficulties, and their analysis performed using the spin-Hamiltonian methodology, although rhombicity of the zfs tensor needs to be taken into account.

In our study, we have focused on a simple complex of HS Fe^{2+}, namely, the hexaaqua ion. Tregenna-Piggott and co-workers have published a number of excellent HFEPR and INS studies on a variety of hexaaqua paramagnetic 3d block ions, such as V^{3+} ($3d^2$, $S = 1$),[27–29] Cr^{2+} ($3d^4$, $S = 2$),[30] and Mn^{3+}.[24] Their preferred form of the hexaaqua ions have been either the alums (general formula: $M'M(SO_4)_2{\cdot}12H_2O$, where M′ = 1+ cation: group 1 metal ion, ammonium, etc., and M = 3+ cation: Al^{3+}, transition metal ion, etc.) or the Tutton's salts (general formula: $M'_2[M(H_2O)_6](SO_4)_2$, where M′ = 1+ cation, M = 2+ cation). We have also chosen for this study a Tutton's salt of iron, $(NH_4)_2[Fe(H_2O)_6](SO_4)_2$, historically referred to as ferrous ammonium sulfate, and widely used in analytical chemistry as a stable source of soluble Fe^{2+}. This complex is shown in Fig. 2, based on the reported crystal structure.[31] We have also selected another salt: ferrous perchlorate hydrate, $[Fe(H_2O)_6](ClO_4)_2$.

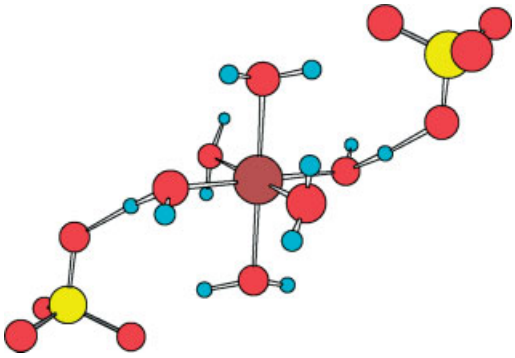

Figure 2. Room-temperature structure of $(NH_4)_2[Fe(H_2O)_6](SO_4)_2$ based on the work of Montgomery *et al.*[31] Ammonium ions are not shown.

Although $[Fe(H_2O)_6](ClO_4)_2$ is not as stable toward oxidation as the other complex, the present study of this salt will be seen to be more informative in terms of the quality of FDMRS, HFEPR, and magnetic susceptibility data than that of $(NH_4)_2[Fe(H_2O)_6](SO_4)_2$. The X-ray crystal structure of $[Fe(H_2O)_6](ClO_4)_2$ has been reported; however, this compound shows twinning, so that the structure is less satisfactory than that of the other complex.[32]

In addition to magnetic resonance methods, we also include powder DC magnetic susceptibility and zero-field Mössbauer effect spectroscopy measurements. DC magnetic susceptibility has historically been used to investigate non-Kramers transition metal ions where EPR failed,[33] and can still help determine the overall spin magnitude, S, as well as independently verify the spin-Hamiltonian parameters obtained from FDMRS and HFEPR. Zero-field Mössbauer spectroscopy allows ready determination of the nature of the orbital ground state that arises from the ^5D free-ion configuration and may also serve to check the gross purity of the samples, in particular, for the presence of oxidation products such as Fe^{3+}.

EXPERIMENTAL

Materials

The hexaaqua Fe^{2+} salts were obtained from commercial sources: $[Fe(H_2O)_6](ClO_4)_2$ from Alfa Aesar and $(NH_4)_2[Fe(H_2O)_6](SO_4)_2$ from Fisher Scientific. Of the many readily available salts of Fe^{2+}, the latter complex is among the most stable toward air oxidation and moisture; however, the perchlorate salt is very hygroscopic and much more readily oxidized to Fe^{3+}, so precautions were taken to prevent these processes, such as use of an argon-filled glove bag during sample grinding and handling.

FDMRS

FDMRS spectra were recorded on plane-parallel pressed powder samples of $[Fe(H_2O)_6](ClO_4)_2$ (thickness (d) = 1.676 mm, mass (m) = 277.1 mg) and $(NH_4)_2[Fe(H_2O)_6](SO_4)_2$ (d = 1.670 mm, m = 259.9 mg) at frequencies ν = 30 GHz – 1.2 THz (quantum energy: 1–40 cm^{-1}), temperatures T = 1.7–300 K, and magnetic fields B = 0–7 T, using a CW THz spectrometer that has been described in the literature.[14] For higher frequencies, a Bruker IFS 113v Fourier-Transform infrared (FTIR) spectrometer equipped with a mercury lamp as a light source was used along with a 50-mm Mylar beam splitter, an Infrared Labs pumped Si bolometer, and a 5-mm aperture. The sample was placed in a home-built zero-field cryostat, or an Oxford Instruments Spectromag 4000 8 T split coil magnetic cryostat with specially enlarged Mylar windows.

HFEPR

HFEPR spectra were recorded on a spectrometer that is part of the Millimeter and Sub-mm Wave Spectroscopy Facility at NHMFL.[34] Tunable frequencies in the 150–700 GHz range (~5–23 cm^{-1} energy) were provided by a set of four BWOs (purchased from the Institute of General Physics, Moscow, Russian Federation). The high-voltage power supply and the permanent magnet housing for the tubes were acquired from the same source. The frequency was precalibrated using a Fabry-Pérot resonator. The magnet used was the resistive magnet (0–25 T) of improved homogeneity (12 ppm in 1-cm diameter spherical volume) and temporal stability. The field was precalibrated using an NMR probe, and checked during the experiment using a (2,2-diphenyl-1-picrylhydrazyl) (DPPH) marker. The oversized-pipes wave propagation system was home-built along the principles outlined before.[35] Detection was provided by a liquid helium-cooled InSb hot-electron bolometer (QMC Ltd., Cardiff, UK). Modulation for detection purposes was provided alternatively by chopping the sub-THz wave beam at *ca* 300 Hz, or by modulating the magnetic field (1 kHz frequency, 2 mT max. amplitude). A Stanford SR830 lock-in amplifier converted the modulated signal to DC voltage.

Typically, 30–40 mg of ground solid sample was used for HFEPR. The sample was kept under a layer of Apiezon grease to slow down a possible oxidation. Since we initially encountered the problem of 'pseudo-noise' (see the 'Results' section), we attempted to prevent or at least minimize field-induced torquing effects by containing the sample in *n*-eicosane mull, or by utilizing pressed KBr pellets of the samples. Only the pellet pressing was successful to a limited degree; the ideal powder-pattern spectra were thus not achieved for any of the investigated salts. However, the tunable-frequency methodology employed here allowed us to identify particular turning points within the nonideal powder patterns and to accurately determine spin-Hamiltonian parameters.

HFEPR analysis

To analyze the EPR spectra, we applied the usual spin Hamiltonian for an S = 2 spin state including the second-order zfs terms:[33]

$$\mathcal{H} = \beta B \cdot \mathbf{g} \cdot S + D(S_z^2 - S(S+1)/3) + E(S_x^2 - S_y^2), \quad (1)$$

where β is the Bohr magneton.

Although fourth-rank zfs terms have been successfully extracted for another quintet spin system, Mn^{3+},[36] this turned out to be impossible in Fe^{2+}, primarily because of the large linewidths and generally lower data quality than in Mn^{3+}

complexes, but also because of a much larger magnitude of D and E. Thus, including fourth-rank terms $B_4{}^iO_4{}^i$ ($i = 0$, 2, 4) did not improve the quality of the fits. The zf energy levels resulting from the spin Hamiltonian (Eqn 1) acting on quintet state wavefunctions are shown in Fig. 1. A spin Hamiltonian for $S = 2$ can also include higher order field-dependent (Zeeman) terms, such as $B \cdot S^3$, which can complicate determination of g-values; however, we did not consider such terms here.

Upon finding by trial-and-error method, the initial (seed) parameters **g**, D and E that gave reasonable simulations; all transitions observed in the experimental powder spectra were identified as corresponding to the x, y, or z turning points. A two-dimensional array whose rows contained frequency, polar angles Θ and Φ, and resonance field was used as our input data. This array was simultaneously fitted by use of a nonlinear least-squares (Simplex) method to minimize the function:

$$\chi^2 = \sum_{i=1}^{N} (f_i^{(\mathrm{calc})} - f_i^{(\mathrm{exp})})^2 \qquad (2)$$

where f_i are the calculated and experimental resonance fields. Because we assumed (and confirmed in separate experiments[35]) that all experimental resonance fields bear approximately the same uncertainty, there was no need to include uncertainties σ_i^2 in the denominator. The resonance fields, $f_i^{(\mathrm{calc})}$ were evaluated using the Householder method.[37] The least-squares procedure was carried out in conjunction with human judgment, which was used to eliminate mathematically possible, but unphysical, results to obtain best-fit parameters for the entire field vs energy 2-D array of EPR transitions. After convergence had been achieved, the Hessian matrix H was calculated.[36] Errors in the best-fit parameters were finally estimated as:

$$\sigma_i = \sqrt{\frac{\chi^2}{N-P}(H^{-1})_{ii}} \qquad (3)$$

where N is the number of experimental resonance fields and P is the number of fitted parameters.

Magnetic susceptibility and Mössbauer spectroscopy

Magnetization measurements were performed using a Quantum Design Co. MPMS Superconductivity Quantum Interference Device (SQUID) magnetometry system over the range 1.8–300 K for fields up to 5 T. The temperature dependence of the susceptibility was obtained in a field of 0.1 T for unground, zero-field cooled, polycrystalline samples.

Magnetic susceptibility data were fitted using a locally written program employed previously.[38] The same spin Hamiltonian as in Eqn 1 was employed together with a powder averaging of orientations and nonlinear least-squares fitting. Data were fitted with both axial and rhombic models ($E \equiv 0$, $E \neq 0$, respectively) and with both isotropic and axial g-values. Although determination of the sign of axial zfs is difficult from this technique, fits with D constrained to be negative were much less successful than those with $D > 0$.

The Mössbauer effect spectra were determined using a conventional constant acceleration spectrometer operated in a multichannel scaling mode. The γ-ray source consisted of 60 mCi of ^{57}Co in a rhodium metal matrix that was maintained at ambient temperature. The spectrometer was calibrated using a 6-μm thick natural abundance iron foil likewise maintained at ambient temperature. The isomer shifts (relative to the center of the magnetic hyperfine pattern of the latter foil and quadrupole splitting) agree well with previous literature values. The linewidths of the innermost pair of $\Delta M_I = \pm 1$ transitions of the latter Zeeman pattern were reproducibly determined to be 0.214 mm/s. Sample temperature variation was achieved using a standard exchange gas liquid helium cryostat (Cryo Industries of America, Inc.) with temperature measurement and control based on silicon diode thermometry in conjunction with a 10 μA excitation source (Lakeshore Cryotronics, Inc). Spectra were fit to unconstrained Lorentzians using the program Origin (Originlab Corporation).

RESULTS

Frequency-domain magnetic resonance spectroscopy (FDMRS)

The FDMRS spectra depicted in Fig. 3 show in general two features. One is an oscillation in the baseline, which

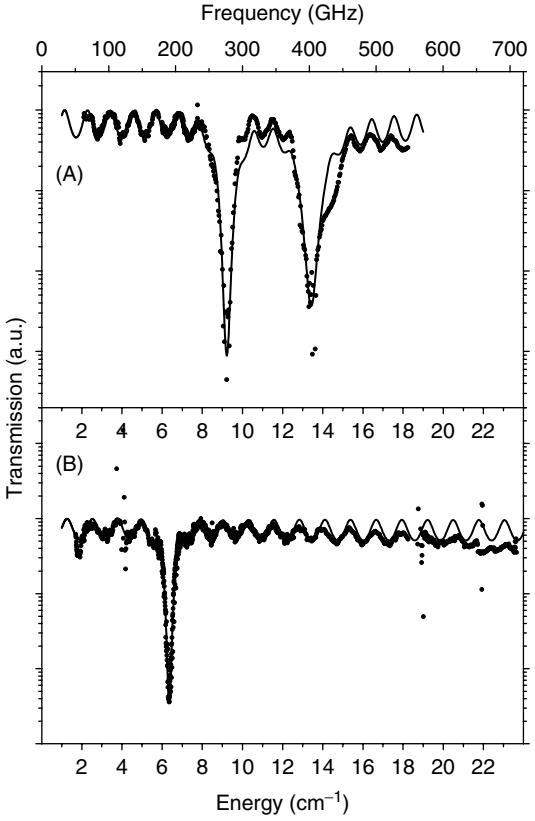

Figure 3. Zero-field FDMRS spectra at 5 K: (A) $[Fe(H_2O)_6](ClO_4)_2$ and (B) $(NH_4)_2[Fe(H_2O)_6](SO_4)_2$. The symbols represent experimental points, while the curves were simulated as described in the 'Results' section.

is caused by Fabry-Pérot like resonances within the plane-parallel sample. These oscillations are fully determined by the complex dielectric permittivity ε^* and the thickness d of the sample. In the analyses, the dielectric constant was fit to the spectra at high temperatures, where magnetic resonance lines are absent. The parameters so derived are then kept constant throughout the fitting process. The second feature is the narrow resonance lines. The magnetodipolar nature of the corresponding transitions is proven by their magnetic-field dependence. The resonance positions are determined using Lorentzian or Gaussian magnetic oscillators in combination with the dielectric parameters.

[Fe(H$_2$O)$_6$](ClO$_4$)$_2$

Figure 3(A) shows the FDMRS spectrum recorded for $[Fe(H_2O)_6](ClO_4)_2$, which contains two resonances, at 9.18 ± 0.02 and $13.43 \pm 0.02\ cm^{-1}$. The intensities of both these lines are maximal at lowest temperature, indicating that they belong to transitions from the lowest-energy M_S state. The use of an FTIR spectrometer allowed the observation of two further resonances at higher energy: 31.44 ± 0.02 and $35.65 \pm 0.02\ cm^{-1}$ (not shown). A much more intense feature is observed at *ca* $46\ cm^{-1}$ (not shown), but can be attributed to phonon absorption in view of its lack of magnetic-field dependence. By assuming a similarity of the spin-Hamiltonian parameters for the $[Fe(H_2O)_6]^{2+}$ ion in $[Fe(H_2O)_6](ClO_4)_2$ with those in $[Fe(H_2O)_6]SiF_6$,[12] all these zf resonances can be combined into a single set of transitions within the ground $S = 2$ state of the complex. Within this framework, the observed resonances correspond to the following transitions: $(D - 3E)$: $9.18\ cm^{-1}$; $(D + 3E)$: $13.43\ cm^{-1}$; $(3D - 3E)$: $31.44\ cm^{-1}$; $(3D + 3E)$: $35.65\ cm^{-1}$. (Each of these four transitions is actually split into two by the factor $3E^2/D$; however, since the zfs tensor is almost axial, the resulting splitting is below the resolution threshold.) A least-square fit yields the following set of zfs parameters: $D = 11.17$ and $E = 0.70\ cm^{-1}$.

(NH$_4$)$_2$[Fe(H$_2$O)$_6$](SO$_4$)$_2$

A strong zf resonance was observed by FDMRS in $(NH_4)_2[Fe(H_2O)_6](SO_4)_2$, at $6.36 \pm 0.02\ cm^{-1}$, as shown in Fig. 3(B). Another resonance was detected near $22.3\ cm^{-1}$ but only at applied magnetic fields (not shown). Since the latter value is only approximate, we did not attempt to estimate zfs parameters from the FDMRS spectra alone.

High-frequency and high-field EPR (HFEPR)

[Fe(H$_2$O)$_6$](ClO$_4$)$_2$

A typical HFEPR spectrum of $[Fe(H_2O)_6](ClO_4)_2$ acquired at 225 GHz is shown in Fig. 4(A). The top trace was recorded using optical modulation on a sample that was ground and contained under Apiezon. The spectrum shows two strong steps 'up' in absorption at low field (1.5 and 3.4 T, respectively) and a weaker step 'down' at 20.4 T. The peak at 8 T appears near $g = 2.00$ and is due to a small amount of Fe^{3+} impurity. Using conventional magnetic modulation reproduces the above features in a derivative representation (middle trace in Fig. 4A), but at the same time amplifies the 'pseudo-noise' appearing between the second and third

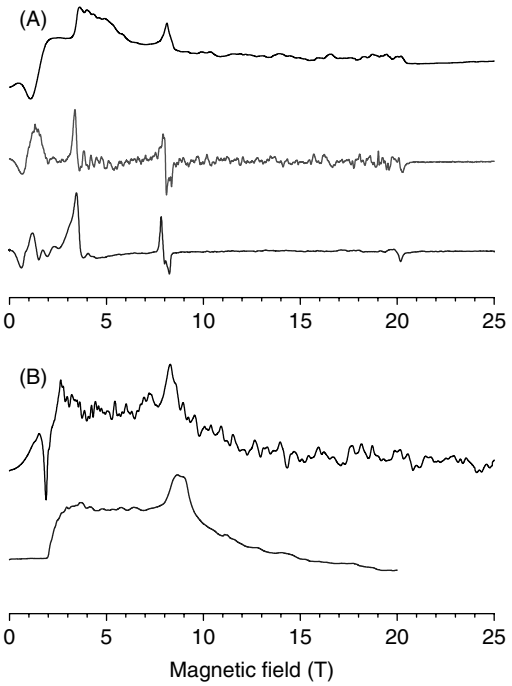

Figure 4. HFEPR spectra at 4.5 K: (A) $[Fe(H_2O)_6](ClO_4)_2$ at 225 GHz. Top trace: optically modulated spectrum of an unrestrained sample; middle trace: magnetically modulated spectrum of the same sample; bottom trace: magnetically modulated spectrum of a KBr pellet. The peak at 8 T is due to a ferric impurity; (B) $(NH_4)_2[Fe(H_2O)_6](SO_4)_2$ at 307 GHz using optical modulation. Upper trace: spectrum of an unrestrained sample; lower trace: spectrum of a pellet.

absorption edges. This phenomenon is due to a finite number of crystallites present in the sample, which do not fully average in space but produce individual peaks in absorption, and this has been observed before.[39] Normally, this problem is alleviated by reducing the crystallite size by grinding. In the case of $[Fe(H_2O)_6](ClO_4)_2$, however, grinding alone did not smooth out the spectra, which suggests a conglomeration of the individual crystallites that might be field induced. It was thus necessary to constrain the sample in a KBr pellet (bottom trace in Fig. 4A), but even this procedure did not produce perfect powder patterns. In general, the overall shape of absorption, which is clearly recognizable from the optically modulated spectrum, is not well reproduced in the low-field region when magnetic modulation is employed. In particular, we found that resonances appearing at, or near, zero field were seriously deformed. In further experiments, we thus exclusively used optical modulation.

Since the interpretation of imperfect powder patterns obtained in single-frequency spectra is a tremendous challenge, in order to extract the relevant information on the spin Hamiltonian of our spin system we performed a tunable-frequency experiment. The results of this experiment are shown in Fig. 5(A). The squares represent the features observed in single-frequency spectra, while the curves were plotted using spin-Hamiltonian parameters best-fit *simultaneously* to the complete 2-D (field vs energy) dataset. The most recognizable feature in Fig. 5(A) is the zf resonance

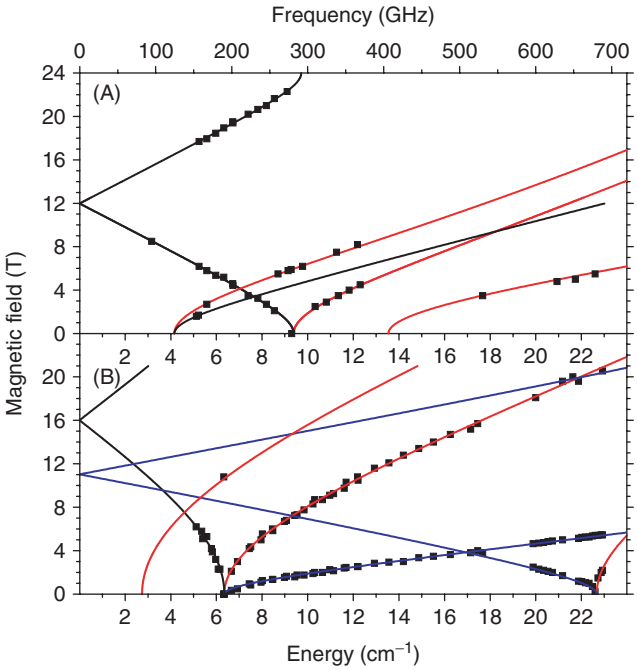

Figure 5. Field vs energy dependence of EPR resonances: (A) $[Fe(H_2O)_6](ClO_4)_2$ and (B) $(NH_4)_2[Fe(H_2O)_6](SO_4)_2$, at 4.5 K. The squares are experimental points while the curves were simulated using best-fitted spin-Hamiltonian parameters given in Table 1. Red curves: turning points with $B_0 \| x$; blue curves: turning points with $B_0 \| y$; black curves: turning points with $B_0 \| z$. For clarity purposes, only those turning points that actually show up in experiment were simulated.

we observed at ~280 GHz (9.3 cm^{-1}). Additionally, the presence of two further zf resonances at *ca* 4 and 13 cm^{-1} can be deduced by extrapolating low-field resonances observed at 4–6 and 18–23 cm^{-1} respectively, to zero field. The resonances at ~9.3 and 13 cm^{-1} are obviously the same as observed in FDMRS spectra at 9.18 and 13.43 cm^{-1}. The low-frequency zf resonance extrapolated at ~4 cm^{-1} does not find its equivalent in the FDMRS response. Since the attribution of zf resonances in FDMRS spectra needed to be confirmed, and no **g**-matrix values could be obtained from zf experiments, we performed a least-squares fit to the complete array of HFEPR resonances, and obtained the following spin-Hamiltonian parameters: $D = +11.34(4)$, $E = +0.69(1)$ cm^{-1} with $g_\perp = 2.18(1)$ and $g_\| = 2.023(6)$. The agreement between experimental features and curves simulated using the best-fitted parameters, as well as among HFEPR, FDMRS, and susceptibility (see below) values, fully confirm the original assignment of the zf resonances, while at the same time refining their values and adding accurate **g**-matrix elements. (The fact that some turning point branches show many more transitions than others is due to problems with the 'pseudo-noise'. Also, the probability of a given transition is not taken into consideration but generally varies with frequency/field). These g-values are similar in magnitude and order to those observed by HFEPR for $[Fe(btz)_2(SCN)_2]$:[25] $g_x = 2.147$, $g_y = 2.166$, $g_z = 2.01$ with the slightly larger deviation from $g = 2.00$ for $[Fe(H_2O)_6](ClO_4)_2$ being attributable, qualitatively, to the weaker ligand field in the hexaaqua complex relative to that in $[Fe(btz)_2(SCN)_2]$, and thus a greater orbital contribution to the observed g-values.

$(NH_4)_2[Fe(H_2O)_6](SO_4)_2$

HFEPR spectra of $(NH_4)_2[Fe(H_2O)_6](SO_4)_2$ display the same general characteristics as those of $[Fe(H_2O)_6](ClO_4)_2$. A typical HFEPR spectrum using optical modulation is shown in Fig. 4(B) as the top trace. The problem of 'pseudo-noise' was only partly solved by pressing a KBr pellet from the ground sample (Fig. 4B, bottom trace). Moreover, pressing the pellet broadened the important features in the spectra (such as the negative dip at 2 T, indicating a turning point in a powder spectrum), making their recognition more difficult than in the unrestrained sample. Given the problems with magnetic modulation outlined above, which tends to amplify the 'pseudo-noise' while obscuring relevant features of the powder pattern, we did not use this method and employed exclusively optical modulation.

We then performed a tunable-frequency experiment on both restrained and unrestrained samples. The data from this experiment are presented as squares in Fig. 5(B). A prominent feature of the field vs energy dependencies shown in Fig. 5(B) is the two zf resonances at *ca* 190 GHz (6.33 cm^{-1}) and 678 GHz (22.6 cm^{-1}) respectively. The former clearly corresponds to the zf transition observed at 6.36 cm^{-1} by FDMRS, while that at high-energy appears in field domain FDMRS, but not in zero field.

Since the two zf resonances appear at energies far below, and above, respectively, the transitions observed both in $[Fe(H_2O)_6](ClO_4)_2$ by us, and in $[Fe(H_2O)_6]SiF_6$ by Champion and Sievers,[12] the spin-Hamiltonian parameters of the $[Fe(H_2O)_6]^{2+}$ ion in $(NH_4)_2[Fe(H_2O)_6](SO_4)_2$ must be very different from the other two systems. We therefore had to search for the assignments of the resonances, and thus also the seed zfs parameters for the computer fit program, by trial and error. The only possible good agreement between experiment and simulation was achieved by assuming a significant rhombicity of the zfs tensor and assigning the 6.36 cm^{-1} resonance to the $(D - 3E + 3E^2/D)$ transition, and the 22.6 cm^{-1} resonance to the $6E$ transition. This assignment results in approximate values of zfs parameters equal to $D = 15$ and $E = 3.8$ cm^{-1}, which were further refined by a simultaneous fit to all resonances to yield the values of $D = +14.94(2)$, $E = +3.778(2)$ cm^{-1} with $g_x = 2.226(6)$, $g_y = 2.31(1)$ and $g_z = 1.93(3)$. The overall agreement of both the zf and high-field resonances with simulations is very satisfactory even if the parameters themselves are quite remarkable because of the high rhombicity of the zfs tensor (see the 'Discussion' section). Additionally, the g-values for $(NH_4)_2[Fe(H_2O)_6](SO_4)_2$ are surprisingly different from those observed for both the perchlorate and for $[Fe(btz)_2(SCN)_2]$ (where consensus values are: $g_\perp = 2.16(2)$, $g_\| = 2.02(1)$): $g_\perp$ is very large and $g_\|$ is very small – less than 2.00 – which is unexpected for a greater than half-filled d shell. It should be pointed out here, however, that $g_\|$ is strongly statistically correlated with D, presumably owing to relatively large uncertainties in the measured resonance fields. Also, the number of experimental points with $B \| z$ is rather limited. The unusual spin-Hamiltonian parameters

for $(NH_4)_2[Fe(H_2O)_6](SO_4)_2$ will require a detailed analysis beyond the scope of this study.

Magnetic susceptibility

Powder DC magnetic susceptibility measurements were made on each complex for corroboration of the magnetic resonance techniques. The temperature dependence of the magnetic susceptibility represented in terms of the effective magnetic moment μ_{eff} is shown in Fig. 6. The room-temperature values of μ_{eff} between 5 and 6 for both salts are approximately those expected for the $S = 2$ ground state. The large drop of μ_{eff} at low temperature in both salts is a strong indication of large zfs, with a magnitude on the order of 10 cm^{-1}. In the case of $[Fe(H_2O)_6](ClO_4)_2$, there is also a distinct step in the temperature dependence of μ_{eff} for at ~270 K (not shown), which is an indication of the well-known order/disorder transition of this material (as a result, susceptibility data for this complex were fit only for temperatures below 250 K. For both complexes, the magnetic moment data in the range 60–250 K are essentially constant and thus Fig. 6 displays only data <80 K), while the anomaly at ~60 K in the same sample is due to molecular oxygen. The experimental points were fitted using the spin Hamiltonian in Eqn 1; the results are presented in Table 1.

For $[Fe(H_2O)_6](ClO_4)_2$, the fit to the magnetic susceptibility data yields values for all the spin-Hamiltonian parameters in good agreement with those determined by both magnetic resonance techniques; a consensus set of parameters among all three techniques is as follows: $D = 11.4(2)$ cm^{-1}, $E = 0.9(3)$ cm^{-1}, and $g_{iso} = 2.13$ (also Table 1). This agreement is especially significant given that determination of E by powder magnetometry is difficult due to the relatively small effect of this interaction on the bulk moment. Correspondingly, use of the HFEPR-determined parameters provides a good fit to the experimental susceptibility data, as shown by the cyan curve in Fig. 6.

For $(NH_4)_2[Fe(H_2O)_6](SO_4)_2$, the fit to the magnetic data is much less successful in that zfs parameters are very different from those obtained from magnetic resonance result (Table 1). Use of the zfs parameters obtained from HFEPR, on the other hand, with independently varying axial g-values, fits the data very adequately (Fig. 6, magenta curve), although the resulting g-values are far from ideal (Table 1). That the $g_\perp$ value is very large and the $g_\parallel$ is very small is in qualitative agreement with the HFEPR results; however, we currently have no explanation for the actual g-values. The magnetic data for $(NH_4)_2[Fe(H_2O)_6](SO_4)_2$ serve as an example of the difficulty of extracting spin-Hamiltonian parameters from a single, bulk measurement. It is likely that multiple-field

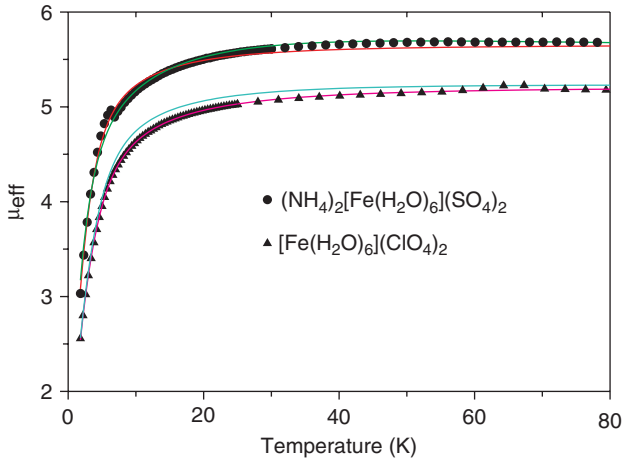

Figure 6. Temperature dependence of the effective magnetic moment (at $H_{applied} = 0.1$ T) for $(NH_4)_2[Fe(H_2O)_6](SO_4)_2$ (data points shown as circles; independent fit given by red curve; fit to zfs values determined by HFEPR with independently variable axial g-values given by green curve) and $[Fe(H_2O)_6](ClO_4)_2$ (data points shown as upwards triangles; independent fit given by magenta curve; fit to all parameters determined by HFEPR given by cyan curve). Spin-Hamiltonian parameters for the fit curves are given in Table 1. Data above 80 K are not shown, as they are essentially constant in effective magnetic moment.

Table 1. Spin-Hamiltonian parameters for the complexes containing $[Fe(H_2O)_6]^{2+}$

Complex	D (cm^{-1})	E (cm^{-1})	g_x	g_y	g_z
$[Fe(H_2O)_6](ClO_4)_2$[a]	+11.17	+0.70	–	–	–
$[Fe(H_2O)_6](ClO_4)_2$[b]	+11.34(4)	+0.69(1)	2.18(1)	2.18[f]	2.023(6)
$[Fe(H_2O)_6](ClO_4)_2$[c]	+11.58	+1.18	2.13	2.13	2.13
$(NH_4)_2[Fe(H_2O)_6](SO_4)_2$[b,d]	+14.94(2)	+3.778(2)	2.226(6)	2.31(1)	1.93(3)
$[Fe(H_2O)_6]SiF_6$[e]	+11.78	+0.67	–	–	–

[a] This work, using FDMRS.

[b] This work, using HFEPR.

[c] This work, using magnetometry; g-values assumed isotropic and D, $E > 0$. For $[Fe(H_2O)_6](ClO_4)_2$, best-fit parameters allowing for axial g-values are: $D = 11.28$ cm^{-1}, $E = 1.05$ cm^{-1}, $g_\perp = 2.11$, $g_\parallel = 2.18$ (which give $g_{iso} = 2.13$).

[d] Magnetometry gave $D = 8.51$ cm^{-1}, $E = 0$ cm^{-1}, $g_{iso} = 2.31$. However, a fit using the D, E values fixed at those determined by HFEPR, with independently variable axial g-values, was essentially indistinguishable from the fully variable fit (Fig. 6). The resulting g-values were: $g_\perp = 2.49$, $g_\parallel = 1.67$ (which give $g_{iso} = 2.22$).

[e] Data from FDMRS study by Champion and Sievers.[12]

[f] g_y was assumed equal to g_x since no experimental data for $B_0 \| y$ were available.

variable-temperature measurements (equidistantly sampled on a 1/T scale) would be more reliable than a single-field measurement; however, the quality of HFEPR data does not justify such measurements, which remain outside the scope of the present work.

Mössbauer effect spectroscopy

The zero-field Mössbauer effect spectra of both samples at 77 K are shown in Fig. 7. They are characteristic for HS Fe^{2+}. A variety of zero- and applied-field Mössbauer spectroscopy studies of $[Fe(H_2O)_6](ClO_4)_2$ and related systems have been published.[40,41] These show that the orbital ground state of these compounds at low temperatures is the orbital singlet, $^5A_1$ (based on d_{z2}, the so-called t_{2g}^0 orbital in *trigonal quantization*).[42] This orbital assignment is based on the magnitude, temperature dependence, and sign of the principal component of the electric field gradient tensor derived from the Mössbauer spectroscopy investigations.

At low temperatures (<4.2 K), Mössbauer spectra of both salts give no evidence of magnetic hyperfine splitting or broadening owing to slow paramagnetic relaxation effects. This is fully consistent with the nonmagnetic singlet spin ground state, $\langle S, M_S| = \langle 2, 0|$, and thus points to a positive D-value, in concert with HFEPR. Furthermore, since $m_L = 0$ for the t_{2g}^0 orbital, the basic spin-only approach to the total ground state magnetism of these paramagnets, i.e. orbital plus spin, used in this paper is entirely appropriate. Similar detailed Mössbauer spectroscopy studies of $(NH_4)_2[Fe(H_2O)_6](SO_4)_2$[43] confirm distortion of the octahedron to the *orbitally nondegenerate* $^5B_2$ based on the d_{xy} tesseral (real d orbital) representation.

The spectra do not show any presence of oxidation products, notably Fe^{3+}, although HFEPR detected a small amount of Fe^{3+} impurity in the less stable of both salts, $[Fe(H_2O)_6](ClO_4)_2$. We have shown previously that HFEPR is more sensitive to the presence of very low levels (<0.5%) of Fe^{3+} than Mössbauer effect spectroscopy if the Fe^{3+} resonance is largely isotropic.[25]

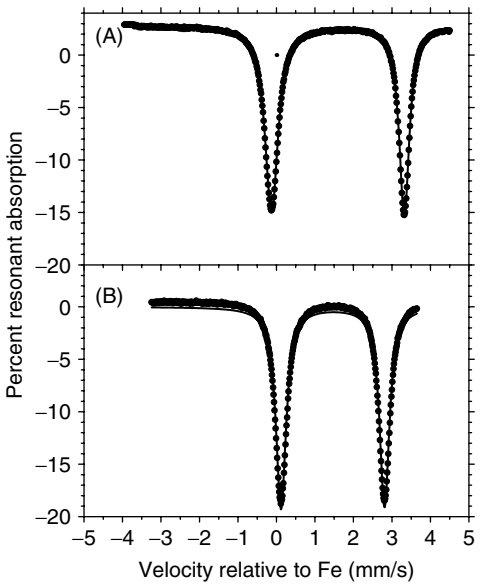

Figure 7. Zero-field Mössbauer effect spectra at 77 K: (A) $[Fe(H_2O)_6](ClO_4)_2$ and (B) $(NH_4)_2[Fe(H_2O)_6](SO_4)_2$. The symbols represent experimental points, while the curves were simulated as described in the 'Experimental' section.

DISCUSSION

We have demonstrated that FDMRS and tunable-frequency HFEPR complement each other in the ultimate goal of establishing accurate values of the spin-Hamiltonian parameters for HS Fe^{2+}, in this case in hexaaqua complexes. The optimal starting point is the FDMRS experiment, because this technique, operating in the frequency domain, can more accurately detect zf resonances than HFEPR, which by its nature operates in the magnetic-field domain. (In particular, HFEPR cannot directly detect a zf resonance, but extrapolates high-field resonances to zero field by frequency tuning.) In an ideal case, which is represented here by the $[Fe(H_2O)_6](ClO_4)_2$ salt, FDMRS and HFEPR results are in full agreement. An HFEPR experiment delivers the **g**-matrix values, which cannot be as conveniently and accurately determined from FDMRS. These spin-Hamiltonian parameters for $[Fe(H_2O)_6](ClO_4)_2$ are fully supported by DC susceptibility measurements, which, although a bulk measurement, is a simple and widely available technique and thus deserves a place in the study of such systems.

For $(NH_4)_2[Fe(H_2O)_6](SO_4)_2$, only a single zf resonance was accurately detected using FDMRS, which is not sufficient to calculate the zfs parameters, but its observation, as well as a detection of its counterpart in the high-frequency spectral region in applied fields, improved the accuracy and reliability of the final spin-Hamiltonian parameters obtained from HFEPR.

In terms of the actual spin-Hamiltonian parameters obtained in this study, one might expect that the situation for both hexaaqua salts of Fe^{2+} would be that of an ideal octahedral symmetry, given that these are homoleptic complexes. This is clearly not the case since results quite unlike those for truly cubic Fe^{2+} systems are obtained. Rather than a single EPR resonance at an effective (X-band) g value of ~3.4–3.6, multiple resonances are observed and these are only at high frequencies, whether by HFEPR or FDMRS. Qualitatively, as can be seen in Fig. 2, the aqua ligands are not point charges, rather, due to the C_{2v} point group symmetry of the water molecule, they exhibit a twist angle with respect to the Fe–O bond axis (i.e. the dihedral angle formed by the H-$(O)_a$-H vector and the O_b-Fe-O_c vector of the aqua ligands *cis* ($O_{a,c}$) to the aqua ligand of interest (O_a) is nonzero). Such systems have been discussed in great detail by Tregenna-Piggott and co-workers,[24,27–30,44–47] and will be treated only qualitatively here. The result of the aqua ligand twist is that the $[Fe(H_2O)_6]^{2+}$ complexes are better represented by S_6 point group symmetry, rather than O_h. In terms of a bonding description, as opposed to a symmetry description (i.e. a ligand field rather than crystal-field model), the π-bonding in aqua ligands is highly anisotropic (e.g. $\pi_\parallel = 0$, $\pi_\perp \gg 0$), which can lead to significant axial and rhombic zfs. Additionally, in $(NH_4)_2[Fe(H_2O)_6](SO_4)_2$, there is the added effect of the sulfate ions that are hydrogen-bonded to the axial aqua ligands, thus potentially providing an

additional axial ligand-field distortion. Qualitatively, this coordination effect may be manifested in the larger D-value for $(NH_4)_2[Fe(H_2O)_6](SO_4)_2$, as opposed to the other complex that does not have such direct anion interactions. Of interest is not only the significant variation of D within the nominally identical $[Fe(H_2O)_6]^{2+}$ ion in different salts (ranging from *ca*. 10 to 15 cm^{-1}) but also, if not particularly, the very high rhombicity of the zfs tensor, reaching the E/D-value of *ca* 0.2 in $(NH_4)_2[Fe(H_2O)_6](SO_4)_2$ (the maximum value of this parameter is 0.33, as follows from Eqn 1). It is particularly noteworthy that independent Mössbauer spectroscopy studies of polycrystalline and oriented single crystal samples of $(NH_4)_2[Fe(H_2O)_6](SO_4)_2$ clearly suggest a rhombic environment of the Fe^{2+} ion on the basis of a nonzero asymmetry parameter for its electric field gradient tensor.[43] While our results are in qualitative agreement with those earlier Mössbauer spectroscopy investigations, a more quantitative treatment is necessary, and will follow.

CONCLUSIONS

HFEPR spectroscopy has been developed over the past decade into an important tool for the investigation of transition metal complexes that are not amenable to study by EPR at conventional (lower) fields and frequencies. The original studies involved complexes of Mn^{3+},[16,17] as have many subsequent ones,[9,18–23] although from a biological point of view, the most important HS ion is Fe^{2+}. Nevertheless, HFEPR of this ion proved difficult to obtain, particularly for the six-coordinate (pseudo-octahedral) geometry, and only recently were high signal-to-noise ratio, extensive HFEPR spectra reported for a representative complex.[25] We have now extended HFEPR to two hexaaqua complexes of Fe^{2+}. We have also shown, following results from many years ago that have been dormant,[11,12] that FDMRS can also be successfully applied to these systems, side by side with HFEPR. Indeed, HFEPR, in its tunable-frequency version, and FDMRS complement each other to a large degree.

Of the two complexes studied, $(NH_4)_2[Fe(H_2O)_6](SO_4)_2$ and $[Fe(H_2O)_6](ClO_4)_2$, the latter represents an ideal situation in terms of the ability to obtain high-quality HFEPR and FDMRS data, which are additionally in very good agreement with a much cruder (i.e. bulk, nonresonant) technique, powder DC magnetic susceptibility. The two magnetic resonance techniques gave as consensus values for the perchlorate salt: $D = 11.2(2)\ cm^{-1}$, $E = 0.70(1)\ cm^{-1}$ (along with $g_x = 2.226(6)$, $g_y = 2.31(1)$, and $g_z = 2.023(5)$ from HFEPR alone). The zfs values are in close agreement with those obtained by Champion and Sievers for $[Fe(H_2O)_6]SiF_6$: $D = 11.78\ cm^{-1}$, $E = 0.67\ cm^{-1}$.[12] Both the perchlorate and hexafluorosilicate salts contain the hexaaquairon(II) ion unencumbered by complicated interionic forces such as those present in $(NH_4)_2[Fe(H_2O)_6](SO_4)_2$ (Fig. 2), and thus provide a reference point in spin-Hamiltonian parameters for $[Fe(H_2O)_6]^{2+}$: $D = 11.5(3)\ cm^{-1}$, $E = 0.7(1)\ cm^{-1}$. We anticipate that future studies of HS Fe^{2+} systems, as well as a ligand-field theory treatment will make use of this information.

Acknowledgments

NHMFL is funded by the National Science Foundation through Cooperative Agreement DMR 0084173 and the State of Florida. The W. M. Keck Foundation funded the high-homogeneity resistive magnet. WMR acknowledges NSF-DMR support toward the purchase of SQUID magnetometry instrumentation at Northeastern University. JvS, SV, and MD acknowledge funding received from the German Science Foundation (DFG), which also supported a visit by JT to Stuttgart.

REFERENCES

1. Lippard SJ, Berg JM. *Principles of Bioinorganic Chemistry*. University Science Books: Mill Valley, 1994.
2. Que L Jr. *Physical Methods in Bioinorganic Chemistry: Spectroscopy and Magnetism*. University Science Books: Sausalito, 2000.
3. Hendrich MP, Debrunner PG. *Biophys. J.* 1989; **56**: 489.
4. Münck E, Surerus KK, Hendrich MP. *Meth. Enzym., Part D* 1993; **227**: 463.
5. Lebedev YS. *Appl. Magn. Reson.* 1994; **7**: 339.
6. Brunel L-C. *Physica B* 1995; **211**: 360.
7. Freed JH. *Ann. Rev. Phys. Chem.* 2000; **51**: 655.
8. Smith GM, Riedi PC. *Electron Paramagnetic Resonance*, vol. 18, Gilbert BC, Davies MJ, Murphy DM (eds). Royal Society of Chemistry: Cambridge, 2002; 254.
9. Mantel C, Hassan AK, Pécaut J, Deronzier A, Collomb M-N, Duboc-Toia C. *J. Am. Chem. Soc.* 2003; **125**: 12337.
10. Joyce RR, Richards PL. *Phys. Rev.* 1969; **179**: 375.
11. Brackett GC, Richards PL, Caughey WS. *J. Chem. Phys.* 1971; **54**: 4383.
12. Champion PM, Sievers AJ. *J. Chem. Phys.* 1977; **66**: 1819.
13. Vongtragool S, Gorshunov B, Dressel M, Krzystek J, Eichhorn DM, Telser J. *Inorg. Chem.* 2003; **42**: 1788.
14. van Slageren J, Vongtragool S, Gorshunov B, Mukhin AA, Karl N, Krzystek J, Telser J, Müller A, Sangregorio C, Gatteschi D, Dressel M. *Phys. Chem. Chem. Phys.* 2003; **5**: 3837.
15. Knapp MJ, Krzystek J, Brunel L-C, Hendrickson DN. *Inorg. Chem.* 2000; **39**: 281.
16. Barra A-L, Gatteschi D, Sessoli R, Abbati GL, Cornia A, Fabretti AC, Uytterhoeven MG. *Angew. Chem. Int. Ed. Engl.* 1997; **36**: 2329.
17. Goldberg DP, Telser J, Krzystek J, Montalban AG, Brunel L-C, Barrett AGM, Hoffman BM. *J. Am. Chem. Soc.* 1997; **119**: 8722.
18. Krzystek J, Telser J, Pardi LA, Goldberg DP, Hoffman BM, Brunel L-C. *Inorg. Chem.* 1999; **38**: 6121.
19. Krzystek J, Telser J, Knapp MJ, Hendrickson DN, Aromí G, Christou G, Angerhofer A, Brunel L-C. *Appl. Magn. Reson.* 2001; **23**: 571.
20. Krzystek J, Telser J, Hoffman BM, Brunel L-C, Licoccia S. *J. Am. Chem. Soc.* 2001; **123**: 7890.
21. Krzystek J, Telser J. *J. Magn. Reson.* 2003; **162**: 454.
22. Krzystek J, Yeagle G, Park J-H, Meisel MW, Britt RD, Brunel L-C, Telser J. *Inorg. Chem.* 2003; **42**: 4610.
23. Limburg J, Vrettos JS, Crabtree RH, Brudvig GW, de Paula JC, Hassan A, Barra A-L, Duboc-Toia C, Collomb M-N. *Inorg. Chem.* 2001; **40**: 1698.
24. Tregenna-Piggott PLW, Weihe H, Barra A-L. *Inorg. Chem.* 2003; **42**: 8504.
25. Ozarowski A, Zvyagin SA, Reiff WM, Telser J, Brunel LC, Krzystek J. *J. Am. Chem. Soc.* 2004; **126**: 6574.
26. Carver G, Tregenna-Piggott PLW, Barra A-L, Neels A, Stride JA. *Inorg. Chem.* 2003; **42**: 5771.
27. Tregenna-Piggott PLW, Weihe H, Bendix J, Barra A-L, Güdel H-U. *Inorg. Chem.* 1999; **38**: 5928.
28. Tregenna-Piggott PLW, Spichiger D, Carver G, Frey B, Meier R, Weihe H, Cowan JA, McIntyre GJ, Zahn G, Barra A-L. *Inorg. Chem.* 2004; **43**: 8049.
29. Tregenna-Piggott PLW, Carver G. *Inorg. Chem.* 2004; **43**: 8061.
30. Dobe C, Noble C, Carver G, Tregenna-Piggott PLW, McIntyre GJ, Barra A-L, Neels A, Janssen S, Juranyi F. *J. Am. Chem. Soc.* 2004; **126**: 16639.

31. Montgomery H, Chastain RV, Natt JJ, Witkowska AM, Lingafelter EC. *Acta Crystallogr.* 1967; **22**: 775.
32. Ghosh M, Ray S. *Z. Kristallogr., Kristallgeom., Kristallphys., Kristallchem.* 1981; **155**: 129.
33. Abragam A, Bleaney B. *Electron Paramagnetic Resonance of Transition Ions*. Dover Publications: New York, 1986.
34. Zvyagin SA, Krzystek J, van Loosdrecht PHM, Dhalenne G, Revcolevschi A. *Physica B* 2004; **346**: 1.
35. Hassan AK, Pardi LA, Krzystek J, Sienkiewicz A, Goy P, Rohrer M, Brunel L-C. *J. Magn. Reson.* 2000; **142**: 300.
36. Aromí G, Telser J, Ozarowski A, Brunel LC, Krzystek J. *Inorg. Chem.* 2005; **44**: 187.
37. Press WH, Flannery BP, Teukolsky AA, Vetterling WT. *Numerical Recipes in Pascal*. Cambridge University Press: Cambridge, 1989; 572.
38. Krzystek J, Fiedler AT, Sokol JJ, Ozarowski A, Zvyagin SA, Brunold TC, Long JR, Brunel L-C, Telser J. *Inorg. Chem.* 2004; **43**: 5645.
39. Telser J, Pardi LA, Krzystek J, Brunel L-C. *Inorg. Chem.* 1998; **37**: 5769.
40. Latorre R, Abeledo CR, Frankel RB, Costamagna JA, Reiff WM, Frank E. *J. Chem. Phys.* 1973; **59**: 2580.
41. Reiff WM, Frankel RB, Abeledo CR. *Chem. Phys. Lett.* 1973; **22**: 124.
42. Ballhausen CJ. *Introduction to Ligand Field Theory*. McGraw-Hill: New York, 1962; 99.
43. Greenwood NN, Gibb TC. *Mössbauer Spectroscopy*. Chapman and Hall: London, 1971; 133.
44. Dolder S, Spichiger D, Tregenna-Piggott PLW. *Inorg. Chem.* 2003; **42**: 1343.
45. Tregenna-Piggott PLW, Andres H-P, McIntyre GJ, Best SP, Wilson CC, Cowan JA. *Inorg. Chem.* 2003; **42**: 1350.
46. Tregenna-Piggott PLW, Best SP. *Inorg. Chem.* 1996; **35**: 5730.
47. Basler R, Tregenna-Piggott PLW, Andres H, Dobe C, Güdel H-U, Janssen S, McIntyre GJ. *J. Am. Chem. Soc.* 2001; **123**: 3377.